Plant Physiology Increases the Magnitude and Spread of the Transient Climate Response in CMIP6 Earth System Models

Claire M. Zarakas[1*], Abigail L. Swann[1,2], Marysa M. Laguë[1,3], Kyle C. Armour[1,4], and James T. Randerson[5]

[1] Department of Atmospheric Sciences, University of Washington

[2] Department of Biology, University of Washington

[3] Department of Earth and Planetary Sciences, University of California, Berkeley

[4] School of Oceanography, University of Washington

[5] Department of Earth System Science, University of California, Irvine

Corresponding author email: czarakas@uw.edu

Abstract:

Increasing concentrations of CO_2 in the atmosphere not only influence climate through CO_2's effect as a greenhouse gas but also through its impact on plants. Plants respond to atmospheric CO_2 concentrations in several ways that can alter surface energy and water fluxes and thus surface climate, including changes in stomatal conductance, water use, and canopy leaf area. These plant physiological responses are already embedded in Earth system models, and a robust literature demonstrates that they can affect global-scale temperature. However, the physiological contribution to transient warming has yet to be assessed systematically in Earth system models. Here this gap is addressed using carbon cycle simulations from the 5th and 6th phases of the Coupled Model Intercomparison Project (CMIP) to isolate the radiative and physiological contributions to the transient climate response (TCR). In CMIP6 models, the physiological effect contributes 0.11°C (standard deviation: 0.10°C; range: 0.02 - 0.29°C) of warming to the TCR, corresponding to 5.2% of the full TCR (standard deviation: 4.1%; range: 1.4 - 13.9%). Moreover, variation in the physiological contribution to the TCR across models contributes disproportionately more to the inter-model spread of TCR estimates than it does to the mean. The largest contribution of plant physiology to CO_2-forced warming – and the inter-model spread in warming – occurs over land, especially in forested regions.

1. Introduction

Increasing concentrations of atmospheric CO_2 alter global temperature through both CO_2's role as a greenhouse gas within the atmosphere (radiative effect) and through plants' response to CO_2 at the land surface (physiological effect). Plants respond to atmospheric CO_2 concentrations by regulating their stomata (pores on the leaves which modulate the exchange of CO_2 and water vapor between the leaf and the

atmosphere), changing water use, adjusting canopy leaf area, and ultimately, changing species composition and vegetation cover. These plant physiological responses to higher CO_2 can influence land surface temperature by altering land evapotranspiration, surface albedo, and surface roughness, which are important controls over the fluxes of water and energy between the land surface and the atmosphere. Here we use the term "physiological effect" to encompass the net effect of all plant responses to increasing CO_2, but note that in some past work the term refers solely to the effect of changes in stomatal conductance (e.g. Skinner et al. 2018).

Plant responses to CO_2 modulate land evapotranspiration through two opposing mechanisms. Higher concentrations of CO_2 in the atmosphere provide a larger gradient over which CO_2 diffuses into the interior airspace of leaves. As a result, most plant types close their stomata in response to increasing CO_2 (the stomatal response), thereby decreasing transpiration per leaf area (Field et al. 1995). In contrast, photosynthetic rates in some cases are limited by access to CO_2, and in those cases more CO_2 can lead to higher rates of photosynthesis, dubbed CO_2 fertilization. This directly impacts photosynthetic rates, with higher photosynthesis (and thus higher stomatal conductance) expected as CO_2 concentrations increase. CO_2 fertilization tends to either have no influence on canopy leaf area or to increase canopy leaf area (Norby and Zak 2011; Donohue et al. 2013), which increases transpiration. The physiological effect's net influence on land evapotranspiration therefore depends on the relative magnitude of these two changes (the stomatal response and the leaf area response), as well as the extent to which vegetation influences land-atmosphere interactions in a given region (Lian et al. 2018). Most Earth system models (ESMs; Swann et al. 2016; Lemordant et al. 2018) and field experiments (Hungate et al. 2002; Leakey et al. 2009) suggest that the stomatal response term dominates in areas with moderate to high leaf area, leading to a net decrease in land evapotranspiration. However, future projections of

67 photosynthetic rates, leaf growth rates, and thus transpiration remain highly uncertain
68 (Friedlingstein et al. 2006; Anav et al. 2013; Piao et al. 2013; Smith et al. 2016; Lian et
69 al. 2018).

70 Physiologically-driven reductions in evapotranspiration can warm local land
71 temperatures directly by decreasing evaporative cooling, as well as indirectly through
72 influences on low level humidity, cloud cover, and precipitation. Recent modeling studies
73 have demonstrated that physiologically-driven decreases in land evapotranspiration can
74 reduce cloud cover by decreasing low level relative humidity (Doutriaux-Boucher et al.
75 2009; Andrews et al. 2011, 2012; Arellano et al. 2012; Lemordant et al. 2018), which
76 amplifies regional physiologically-driven warming. If the leaf area response were to
77 dominate over stomatal responses, the resulting increase in evapotranspiration could
78 decrease land temperatures through these same mechanisms. Kooperman et al. (2018)
79 and Langenbrunner et al. (2019) have also found that physiologically-forced drying of
80 the boundary layer can reduce deep convection and allow for greater advective moisture
81 transport out of lowland forest areas in the lower troposphere, demonstrating that the
82 physiological response not only modulates local surface energy fluxes, but also impacts
83 large scale atmospheric dynamics.

84 In addition to influencing land surface temperature by altering
85 evapotranspiration, the plant physiological response to CO_2 can also influence land
86 surface temperature by altering land surface albedo. CO_2 fertilization generally decreases
87 albedo (thereby increasing temperature) by increasing leaf area and, within dynamic
88 vegetation models, by shifting plant functional types from grasses to trees (Bala et al.
89 2006; Andrews et al. 2019). Expansion of forests in boreal and Arctic regions can result
90 in especially large albedo decreases (Betts 2000; Bala et al. 2006; O'ishi et al. 2009;
91 Andrews et al. 2019) because increases in foliage mask bright snow.

92 The global-scale temperature implications of plants' physiological responses to
93 CO_2 have been long acknowledged. Sellers et al. (1996) were the first to quantify
94 physiologically-driven warming by coupling a biosphere model to an atmosphere model,
95 finding that under a doubling of CO_2 the physiological effect increased global land
96 temperature by about 0.3°C and mean global temperature by about 0.1°C. Since then,
97 multiple modeling studies have demonstrated that the plant physiological response tends
98 to increase land temperatures in most modern ESMs on annual timescales (Betts et al.
99 2007; Andrews et al. 2011; Arora et al. 2013; Swann et al. 2016; Lemordant et al. 2016,
100 2018; Arora et al. 2019) and during heatwaves (Lemordant et al. 2016; Skinner et al.
101 2018; Lemordant and Gentine 2019).
102 Because the physiological effect influences surface temperatures, it is therefore
103 relevant to global-scale metrics of climate sensitivity, such as the equilibrium climate
104 sensitivity (ECS) and transient climate response (TCR). From the perspective of the
105 classical radiative forcing-feedback framework (Gregory et al. 2004; Bony et al. 2006;
106 Roe 2009; Boucher et al. 2013), plants' physiological response to increasing CO_2 can be
107 considered to be a forcing – rather than a feedback – on the climate system because by
108 definition plants are responding to changes in CO_2 rather than to the relatively slow
109 changes in global temperature. However, the timescale over which plants respond to
110 increasing CO_2 ranges from on order seconds to decades. The stomatal response is fast;
111 at the leaf level, stomata respond to changing environmental conditions in less than an
112 hour (Vico et al. 2011), and the timescale of the atmospheric adjustment to the stomatal
113 response occurs on the timescale of a few months (Doutriaux-Boucher et al. 2009;
114 Andrews et al. 2011). Doutriaux-Boucher et al. (2009) have demonstrated that this fast
115 stomatal response rapidly reduces low cloud cover and thereby the cloud radiative effect,
116 which has been shown to be an important contributor to global warming and its
117 uncertainty (Geoffroy et al. 2012). The leaf area and plant distribution responses are

slower, occurring on timescales of years to decades (Fisher et al. 2019). Thus, whether the physiological effect will be included in the calculation of radiative forcing depends on the definition used: it would be excluded from the *instantaneous* radiative forcing, which accounts only for the instantaneous impact of CO_2 on the top-of-atmosphere radiation budget; but it would be included in the *effective* radiative forcing, which allows for adjustments to the troposphere, stratosphere, and land surface properties (Sherwood et al. 2015). We will discuss this ambiguity in more detail later, but we focus our analysis on the influence of the physiological effect on the TCR, which is independent of the forcing definition used.

Although plants' physiological responses to CO_2 are already embedded in the ESMs used to estimate the TCR, the physiological effect's contribution to this metric has received limited recognition by the climate dynamics community. While studies focusing on carbon cycle feedbacks have quantified physiologically-driven warming across models as part of disentangling carbon-concentration and carbon-climate feedbacks (e.g. Arora et al. 2013, 2019), studies of the physiological contribution to CO_2-forced warming within a climate dynamics framework have been limited to ESMs from a few individual modeling centers (summarized in Table S1 in the online supplement; Sellers et al. 1996; Betts et al. 1997; Cox et al. 1999; Douville et al. 2000; Levis et al. 2000; Bala et al. 2006; Betts et al. 2007; Doutriaux-Boucher et al. 2009; Boucher et al. 2009; Cao et al. 2009; O'ishi et al. 2009; Cao et al. 2010; Andrews et al. 2011; Pu and Dickinson 2012). Physiology's contribution to the TCR has not been systematically assessed across models and Coupled Model Intercomparison Project (CMIP) phases.

Additionally, past studies have not specifically quantified the physiological contribution to the TCR using the same experimental methodology from which the full TCR is calculated. For example, baseline levels of CO_2 have ranged from 280 to 400 ppm across experiments (Table S1 in online supplemental material) and the

physiological effect's influence on temperature has been analyzed from both abrupt (e.g. Doutriaux-Boucher et al. 2009; Cao et al. 2010; Andrews et al. 2011) and transient (Bala et al. 2006; Boucher et al. 2009) CO_2 perturbations. Modeling studies have also differed in whether they include both the stomatal and leaf area components of the physiological effect or only the stomatal component. While these different experimental designs have provided insights into the mechanisms and timescales of the physiological effect's influence on climate, they do not provide systematic estimates of the full physiological contribution to the TCR across ESMs.

The lack of systematic inter-model comparison of the physiological contribution to the TCR is a problematic gap in the existing literature because past work suggests that physiologically-driven transient warming may differ across models. Models disagree both on how plants respond to increasing CO_2 (Friedlingstein et al. 2006; Anav et al. 2013; Piao et al. 2013; Smith et al. 2016; Lian et al. 2018) and on how the atmosphere responds to perturbations to the land surface energy budget (Andrews et al. 2009; Devaraju et al. 2018). This suggests that inter-model disagreement about the magnitude of physiologically-driven warming may be an unrecognized contributor to inter-model spread in CO_2-forced warming. Additionally, poor model agreement on the magnitude of physiologically-driven warming would mean that an estimate derived from a single model may not capture the true multi-model mean. To address this gap, we use standardized carbon cycle model simulations from the CMIP phase 5 and 6 archives to quantify (1) the magnitude of the physiological effect's influence on temperature across models, (2) whether trends in the physiological effect contribute to the increase in the TCR noted for many recent models (Andrews et al. 2019; Gettelman et al. 2019; Golaz et al. 2019; Flynn and Mauritsen 2020), (3) the spatial pattern of physiologically-driven temperature changes, (4) how physiological processes contribute to variability in multi-

model estimates of the TCR, and (5) the mechanism through which the physiological effect influences temperature.

2. Methods

2.1. CMIP Experiments

As part of CMIP5 and CMIP6, modeling groups performed three concentration-driven experiments (summarized in Table 1) in which CO_2 concentrations increase by 1 percent per year from pre-industrial levels (284.3 ppm) to a quadrupling of CO_2 (1144.9 ppm), while all other forcings remain at pre-industrial levels. The spatial pattern of vegetation in these simulations comes from the pre-industrial era; this spatial pattern remains constant throughout the simulation except for in land models with dynamic vegetation (see Tables S2 and S3 in online supplemental material), where the distribution of plant functional types changes based on climate and resource availability. In one set of simulations, referred to here as 'FULL' (CMIP6 experiment '1pctCO2'), both the atmosphere and carbon cycle (on land and in the oceans) experience increasing CO_2 concentrations. Additional experiments conducted as part of the Coupled Climate–Carbon Cycle Model Intercomparison Project (C4MIP; Friedlingstein et al. 2006; Jones et al. 2016) enable us to isolate how much the physiological and radiative effects of CO_2 each contribute to surface warming. In one set of C4MIP simulations, referred to here as 'RAD' (CMIP6 experiment '1pctCO2-rad'), only the atmosphere experiences increasing CO_2 concentrations, while the terrestrial and oceanic carbon cycles experience constant pre-industrial CO_2 concentrations. In another set of C4MIP simulations, referred to here as 'PHYS' (CMIP6 experiment '1pctCO2-bgc'), the radiative transfer submodels in the atmosphere experience constant pre-industrial CO_2 concentrations, while the land surface and ocean carbon cycle submodels experience the increasing CO_2 concentrations.

194 We use the concentration-driven pre-industrial control experiment (referred to here as
195 'PI', CMIP6 experiment 'piControl') as the baseline from which anomalies are taken.

196 ## 2.2. Models

197 We analyze output from all ESMs that had uploaded near-surface air
198 temperature monthly data for the FULL, PI, and PHYS and/or RAD experiment to the
199 Earth System Grid by January 29, 2020. This consisted of 8 CMIP5 models and 9
200 CMIP6 models (Table 2). These models all include interactive representations of the
201 carbon cycle; plants in these models respond to increasing CO_2 by changing leaf area,
202 stomatal conductance, and, in some models, the location and distribution of plant
203 functional types (Tables S2 and S3 in online supplemental material). Ocean responses to
204 increasing CO_2 include changes in inorganic and biological carbon cycling, which have
205 negligible direct influences on modeled ocean surface temperature. The only potential
206 direct influences of ocean carbon cycle responses on ocean surface temperatures in the
207 PHYS experiments are through changes in plankton community structure which can
208 alter (1) ocean biogeophysical properties and (2) the emission of gases and particles
209 which influence aerosol formation (Hense et al. 2017). These effects are not represented
210 in most models. When multi-model mean maps are reported, they are calculated after
211 smoothly re-gridding model output to a consistent grid.

212 ## 2.3. Calculation of the TCR

213 We calculate the TCR as the change in globally averaged near-surface air
214 temperature during the 20-year window centered on the time of CO_2 doubling (years 61-
215 80 of the simulation where CO_2 concentration increases by 1% per year) relative to pre-
216 industrial CO_2 concentrations. When using the PI experiment as a control, we account
217 for model drift by subtracting the linear trend of PI years 1-140 following Gregory and
218 Forster (2008), where year 1 corresponds to the year at which FULL, RAD, and PHYS

were branched from PI. We refer to the physiological and radiative contributions to the full TCR as TCR_{PHYS} and TCR_{RAD}, respectively.

We assess whether our estimates of physiologically-driven warming are robust relative to variability in the Earth system by comparing TCR_{PHYS} to the distribution of 20-year running mean global temperatures in the full PI control experiments (Figure S1 in the online supplemental material). In two of the CMIP6 models evaluated here (BCC-CSM2-MR and CNRM-ESM2-1), large, multidecadal (greater than 20 year) oscillations exist in the PI control (Figure S1 in the online supplemental material; noted in Parsons et al. (In Revision)). The magnitude of these oscillations greatly exceeds the magnitude of the TCR_{PHYS} signal, and thus we cannot confidently quantify the TCR_{PHYS} for these two models. These models' large multidecadal PI oscillations also have implications for TCR_{FULL}, as they suggest that model TCR_{FULL} estimates may be strongly influenced by variability rather than representing the CO_2-forced warming signal, since for these models smoothing out variability would require an averaging period of greater than 20 years.

2.4. Isolating Physiology's Influence on Temperature

We quantify the influence of the physiological effect in two ways: as the difference between the FULL and RAD simulations (FULL-RAD) and as the difference between the PHYS and PI simulations (PHYS-PI). Both represent physiology's influence on the TCR, but FULL-RAD includes any nonlinear interactions between the radiative and physiological effects of increasing CO_2, while PHYS-PI does not. For example, FULL-RAD would include the interaction between CO_2 fertilization and changes in leaf area (quantified as the leaf area index, LAI) induced by RAD-driven warming. We focus on the FULL-RAD methodology in the main text because it emphasizes how much the physiological effect changes climate relative to what models would otherwise show from radiative forcing alone. Because FULL and RAD branch

from the same point of the PI simulation, FULL-RAD also avoids issues related to drift in the PI control. There is some nonlinearity between the radiative and physiological effects of CO_2, but there is poor model agreement on the sign and spatial pattern of the interaction term (Figures S2 and S3 in the online supplemental material).

2.5. Partitioning Physiological Influences on Evapotranspiration

We partition the total physiologically-driven change in land evapotranspiration into its component physiological drivers according to Equation 1, where the four terms on the right-hand side indicate the land evapotranspiration change due to (1) changes in leaf area, (2) changes in stomatal conductance (approximated as changes in transpiration per leaf area), (3) interactions between changes in stomatal conductance and changes in leaf area, and (4) changes in land evaporation. The derivation of Equation 1 is included in the online supplemental material.

$$\Delta ET = \left(\frac{T}{L}\right)_{RAD} (\Delta L) + L_{RAD}\left(\Delta\frac{T}{L}\right) + \left(\Delta\frac{T}{L}\right)(\Delta L) + \Delta E \qquad \text{Equation 1}$$

where ET = evapotranspiration (mm/day); T = transpiration (mm/day); L = leaf area index (unitless); and E = evaporation (mm/day). The RAD subscript indicates the value from the RAD experiment, and Δ indicates the physiologically-driven change, as calculated from FULL-RAD.

3. Results and Discussion

3.1. Physiology's Contribution to the TCR

The radiative effect of CO_2 is, unsurprisingly, the dominant contributor to the TCR. However, we also find that the physiological response to increased CO_2 has a non-negligible secondary contribution to the TCR in many CMIP5 and CMIP6 models. In CMIP6 models, the physiological effect contributes about 0.11°C (standard deviation:

0.10°C; range: 0.02 - 0.29°C) to the TCR, corresponding to 5.2% of the full TCR (standard deviation: 4.1%; range: 1.4 - 13.9%) (Figure 1a). For a few CMIP6 models (especially UKESM1-0-LL and CESM2), the physiological contribution to warming is quite large, accounting for over 10% of the total TCR. In CMIP5 models (note that a different subset of modeling centers have the necessary CMIP5 model simulations; see Table 2), the physiological effect contributes 0.14°C (standard deviation: 0.16°C; range: 0.00 - 0.51°C) to the TCR, corresponding to 6.6% of the full TCR (standard deviation: 6.3%; range: 0.1 - 20.1%).

When comparing the same subset of six models for which we have model output from both CMIP phases, physiologically-driven warming is comparable in CMIP5 and CMIP6. From CMIP5 to CMIP6, the mean TCR_{PHYS} across these models remained roughly constant (Table 2). TCR_{PHYS} increased for 4 of 6 models (Table 2; Figure 1b), but notably decreased for the model with the highest TCR_{PHYS} in CMIP5 (the Met Office Hadley Centre model, which is HadGEM2-ES in CMIP5 and UKESM1-0-LL in CMIP6). This suggests that the increases in TCR_{FULL} from CMIP5 to CMIP6 noted for many recent models (Andrews et al. 2019; Gettelman et al. 2019; Golaz et al. 2019; Flynn and Mauritsen 2020) were driven primarily by increases in TCR_{RAD} rather than TCR_{PHYS}. Physiology's relative contribution to the TCR decreased in most models (Figure 1a, Table 2), due to many CMIP6 models' increased values of TCR_{RAD}.

The multi-model mean TCR_{PHYS} values reported here are within the range of estimates from other studies (summarized in Table S1 in online supplemental material), but on the low side of this range for two reasons. Firstly, this may relate to publication bias: of the eleven modeling centers included in this analysis, the only two modeling centers that had previously published CMIP5 estimates of physiologically-driven warming at $2xCO_2$ have above average TCR_{PHYS}. Our study is the first to compare TCR_{PHYS} across models, and the fact that the existing literature did not capture the full

spread in TCR_{PHYS} across models underscores the importance of a multi-model approach. A second reason that our multi-model estimate of TCR_{PHYS} is on the low side of previous estimates results from the fact that many previous studies isolated the effect of the stomatal response on near-surface temperatures rather than the net effect of both the stomatal and leaf area response (Table S1 in online supplemental material); we expect a larger temperature increase from the stomatal response alone than from the combined stomatal and leaf area responses because the leaf area response counteracts the stomatal response's influence on evapotranspiration.

The global mean TCR_{PHYS} signal is small in comparison to TCR_{FULL}, and it is statistically significant relative to the pre-industrial control for only 4 of 9 CMIP6 and 5 of 8 CMIP5 models at $2xCO_2$ (Table S4 in online supplemental material). However, the physiologically-driven warming signal increases with increasing CO_2 concentration, reaching a mean of 0.20°C (standard deviation: 0.12°C; range: 0.03 - 0.45°C) by $4xCO_2$ and emerging from the noise (Figure 1b). By $4xCO_2$, physiologically-driven warming is statistically significant for 6 of 9 CMIP6 and 7 of 8 CMIP5 models (Table S4 in online supplemental material). The three CMIP6 models that are not statistically significant by $4xCO_2$ (CNRM-ESM2-1, BCC-CSM2-MR, and IPSL-CM6A-LR) are the three models with the most variability in the PI control of all the CMIP5 and CMIP6 models we analyze. The significant physiologically-driven warming at higher CO_2 concentrations, inter-model agreement in the sign of TCR_{PHYS}, and consistent spatial pattern of warming (detailed in section 3.2) gives us confidence that we are detecting a real physiologically-driven signal and not just picking up internal variability. However, internal variability is a large source of uncertainty in quantifying TCR_{PHYS} (Figure 1b), and this uncertainty is intrinsically included in estimates of TCR_{FULL}. Integration of a large-ensembles approach into the next C4MIP is necessary to address this issue and to

reduce uncertainties in the TCR in future work. This could be done through integrating a requirement for a minimum number of initial condition ensembles in the experiment.

3.2. Spatial Pattern of Physiologically-Driven Warming

The physiological effect only directly influences land surface properties, and thus the largest warming driven by the physiological effect occurs over land. In CMIP6 models, the physiological effect results in a land mean warming of 0.21°C at 2xCO_2 and 0.41°C at 4xCO_2, relative to a corresponding mean ocean warming of 0.07°C and 0.13°C respectively (Figure 2a). Physiologically-driven warming over land is also statistically significant for more ESMs by 2xCO_2 than it is for the global mean (Table S4 in online supplemental material). Because most models do not have any mechanism for the physiological effect of CO_2 to directly warm the oceans, the modelled physiologically-driven warming over oceans must be the result of remote, land driven warming. The spatial pattern of physiologically-driven warming that we find is consistent with other studies, which also show the greatest warming over land and modest ocean warming (Table S1 in online supplemental material).

The greatest mean physiologically-driven warming occurs over boreal forests and non-glaciated high-latitude land, followed by temperate and tropical forested regions. The agreement across models is reasonably high - at least 6 of 9 CMIP6 models agree that the physiological effect results in warming in these three biomes at 2xCO_2, and 8 of 9 CMIP6 models show warming in these biomes at 4xCO_2 (Figures S4 and S5). Relative to radiatively-driven warming, physiology also contributes more to land warming than ocean warming, with physiological forcing constituting a mean 7.3% of total CO_2-forced land warming at 2xCO_2 compared to 4.2% of ocean warming (Figure 2b). The physiological effect therefore amplifies the land/ocean warming contrast: while land warms a mean 1.57 times more than ocean in RAD for CMIP6, the mean land/ocean warming contrast in FULL is 1.62, due to the addition of the physiological effect (Figure

346 3). This physiologically-driven enhancement of the land/ocean warming contrast was
347 previously demonstrated for Met Office Hadley Centre models (Joshi et al. 2008; Dong
348 et al. 2009), and we show here that this warming contrast is robust across most CMIP
349 models (Figure 3).

350 The larger absolute and relative physiologically-driven warming over non-
351 glaciated land is consistent with the physiological effect directly influencing land surface
352 properties in regions with plant cover, while influencing glaciated land and oceans only
353 indirectly through changes in heat transport, clouds, and other aspects of climate
354 dynamics. Though the remote influence of physiological forcing on oceans and glaciated
355 land is relatively modest, most models (8 of 9) agree that the physiological effect results
356 in mean warming of near-surface oceanic air and ocean surface layers. The regions of the
357 most robust physiologically-driven oceanic warming across models are the western North
358 Atlantic, equatorial Pacific, equatorial Indian Ocean, and high latitude Pacific.

359 Byrne and O'Gorman (2018) suggest that increases in the near surface land-ocean
360 temperature contrast are causally driven by temperature change over the ocean.
361 However, the physiologically-driven enhanced land-ocean contrast, where the only initial
362 difference is over the land surface, shows that land surface processes can also initiate the
363 feedback loop of decreasing relative humidity over land leading to a larger increase in
364 temperature over land relative to over ocean. The potential to initiate this loop through
365 land processes is noted by Byrne and O'Gorman (2016), and we further emphasize that
366 point here. It is important to acknowledge the physiological effect's greater relative
367 contribution to land warming because land warming (rather than global mean warming)
368 is the relevant metric for many societal climate impacts.

3.3. Physiology's Contribution to Uncertainty in CO_2-Forced Warming

The magnitude of global physiologically-driven warming varies significantly across models (Figures 1 and 4) and this uncertainty contributes to the inter-model spread of TCR estimates. In the CMIP6 models analyzed here, the radiative effect alone explains about 89% of the standard deviation and 91% of the inter-model range in the TCR (Figure 5), with the physiological effect contributing the remaining 11% and 9%, respectively. The physiological effect contributes more to uncertainty in CO_2-forced warming over land. Averaged across all non-glaciated land, the physiological effect explains about 16% of the standard deviation and 18% of the inter-model range mean land warming at 2xCO_2 in CMIP6 (Figure 5). In some highly forested land regions (tropical Africa, southeastern South America, and the southeastern United States), inter-model disagreement in local warming at 2xCO_2 is driven by approximately equal contributions of uncertainty from physiologically- and radiatively-forced warming (Figure 6). These results suggest that the physiological effect is a non-negligible contributor to inter-model spread in the TCR and regional CO_2-forced warming. However, some of these pre-industrial forested regions, especially southeastern South America, are largely deforested in the present day, which means that in scenario-based future projections the physiological effect may contribute less to uncertainty in these regions than Figure 6 implies.

A limitation of this study is that the C4MIP model output necessary to disentangle physiologically- and radiatively-forced warming is only available for about a quarter of the models for which we can estimate the full TCR (9 of 34 for CMIP6 and 8 of 30 for CMIP5). We therefore cannot quantify TCR_{PHYS}, or the physiological contribution to uncertainty in the TCR, for the remaining CMIP models. Future work could further leverage C4MIP model output to assess whether signatures of

physiologically-driven warming (such as seasonal variations in the CO2-forced change of the diurnal temperature range; Bounoua et al. 1999; Collatz et al. 2000; Leeuwen et al. 2011) could be used to estimate the physiological contributions to mean warming from the FULL experiments alone.

3.4. Mechanism of Physiologically-Driven Warming

3.4.1. Land Mechanism

The physiological effect increases near-surface air temperatures over land by modifying surface properties which modulate terrestrial energy fluxes (Laguë et al. 2019). This occurs through (1) changes in the partitioning between surface turbulent fluxes resulting from physiological influences on evapotranspiration, (2) radiative changes due to physiologically-driven changes in albedo, cloud cover, and column water vapor, and (3) changes in surface roughness resulting from changes in leaf area and vegetation distribution.

In most models, plants' response to CO_2 causes a net decrease in mean land evapotranspiration, especially in the tropics (Figure 7), indicating that stomatal closure decreases evapotranspiration by enough to offset increases in evapotranspiration from increased leaf area, though the magnitude and sign of evapotranspiration change does vary spatially across models. In the CMIP6 multi-model mean at $2xCO_2$, changes in stomatal conductance (approximated by the change in transpiration per leaf area) decreases global land evapotranspiration by 0.14 mm/day (standard deviation: 0.08 mm/day; range: 0.02-0.27 mm/day), global leaf area changes increase evapotranspiration by 0.19 mm/day (standard deviation: 0.15 mm/day; range: 0.00-0.52 mm/day), and the interaction between changes in stomatal conductance and leaf area decreases evapotranspiration by an additional 0.07 mm/day (standard deviation: 0.08 mm/day; range: 0.00-0.29 mm/day; Figure 8). Land evaporation changes minimally (0.00 mm/day; standard deviation: 0.03 mm/day; range: -0.06 - +0.05 mm/day; Figure 8). In

the multi-model mean, the net effect of these physiological responses is a decrease in evapotranspiration, with the largest and most robust decrease in the tropics (Figures 7, 8, and 9). This physiologically-driven decrease in evapotranspiration due to increased CO_2 has previously been documented for CMIP5 models (Swann et al. 2016; Lemordant et al. 2018), and holds for the new CMIP6 models analyzed here. Under constant net radiation at the surface, this physiologically-driven decrease in evapotranspiration results in more energy leaving the land surface through sensible heating (Figure 9), thereby increasing near-surface air temperatures.

The physiological effect also increases surface and near-surface temperatures by increasing the net radiation reaching the surface. Net shortwave radiation on land increases primarily through albedo decreases and changes in cloud cover (Figure 9). Albedo decreases primarily in high latitudes (Figure 7), due to both increases in leaf area and decreases in snow cover due to increased temperatures. Consistent with previous studies (Doutriaux-Boucher et al. 2009; Andrews et al. 2011, 2012; Arellano et al. 2012; Lemordant et al. 2018), downwelling shortwave radiation (SW_{down}) reaching the surface also increases as a consequence of decreases in cloud cover (especially in Northern Hemisphere mid- and high-latitudes and over the northeastern Amazon; Figure 9), which are driven both by decreases in relative humidity from physiologically-forced reductions in evapotranspiration and by increases in air temperatures. Most models show negligible mean changes in clear-sky SW_{down} (which could be modified by changes in water vapor and aerosols), with the exception of UKESM1-0-LL and CanESM5, which show slight decreases in SW_{down}. This result differs from CMIP5, in which the Hadley Centre model was the only model to show physiologically-driven changes in clear-sky SW_{down} , which increased due to vegetation's influence on dust optical depth (Andrews et al. 2012).

The physiological effect also influences surface net longwave radiation (Figure 9) through changes in surface and boundary layer temperatures, cloud cover, atmospheric column water vapor, and the partitioning of surface energy fluxes. Outgoing longwave radiation from the land surface (LW_{up}) increases with increasing surface temperature through the Planck feedback. Warming of the boundary layer (driven by both increased sensible heating and by longwave radiation associated with surface warming) increases downward longwave radiation at the land surface (LW_{down}), partially offsetting the increase in LW_{up} (Vargas Zeppetello et al. 2019). Physiologically-driven decreases in atmospheric water vapor (which is a strong greenhouse gas) decrease LW_{down}, as do cloud changes resulting from reduced land evapotranspiration. The net effect of all of these processes generally results in a decrease of net longwave radiation over most vegetated land.

3.4.2. Ocean Mechanism

Because most models do not have any mechanism for the physiological effect of CO_2 to directly warm the oceans, the modelled physiologically-driven oceanic warming must be the result of remote, land-driven warming. The physiological effect on land can alter ocean temperatures through (1) advection of continental air that has been directly influenced by changes in land surface properties (e.g. changes in air temperature or moisture content) and (2) changes in atmospheric or oceanic circulation. The fact that the most robust oceanic warming regions are downwind of warming land regions suggests that advection of warm continental air is contributing to oceanic warming. Cloud cover over oceans also decreases in some regions that are downwind of land, particularly in the North Atlantic, increasing ocean temperatures by increasing net radiation (Figure 9).

Teleconnections likely also contribute to ocean warming, based on past work indicating that changes in large-scale atmospheric circulation can be induced by

physiological forcing (Kooperman et al. 2018; Langenbrunner et al. 2019) or other changes in land surface properties (Swann et al. 2012, 2014; Devaraju et al. 2015; Laguë and Swann 2016; Devaraju et al. 2018). Additionally, the physiological effect has the potential to induce changes in ocean circulation (e.g. Diffenbaugh et al. 2004). In particular, the pattern of physiologically-driven oceanic warming in the North Atlantic is consistent with a weakening of the Atlantic Meridional Overturning Circulation (AMOC; e.g. Marshall et al. 2015; Caesar et al. 2018). A potential mechanism is that warming of the air advected off the North American continent would reduce the flux of heat from the ocean to the atmosphere in the subpolar North Atlantic, decreasing deep convection.

While the C4MIP experimental design does not enable us to directly quantify the relative contributions of advection and circulation changes to oceanic warming, exploration of the links between land surface perturbations and ocean temperatures merits further research. Recognizing the oceanic component of physiologically-driven warming is important because it constitutes about half of TCR_{PHYS} – even though the magnitude of physiologically-driven oceanic warming is much smaller than land warming on a per area basis, the TCR is a global-scale metric and ocean constitutes about 70% of the Earth's surface area.

4. Conclusions and Implications

4.1. Magnitude of TCR_{PHYS}

The biological and ecological processes governing canopy leaf area and stomatal conductance are often considered to exist squarely in the domain of carbon cycle feedbacks (i.e. they impact the climate system through their influence on CO_2 concentrations themselves). Our analysis demonstrates that these terrestrial carbon

cycle processes are also embedded in global climate sensitivity metrics like the TCR through plants' impact on land surface properties and surface energy fluxes.

We quantified the plant physiological effect's small but significant influence on CO_2-forced temperature changes, finding that at $2xCO_2$ the physiological effect contributes about 0.11°C (5.2%) to the TCR and leads to about 0.21°C of warming over non-glaciated land. To put our results into context, the physiological contribution to the TCR is the same order of magnitude as the surface albedo feedback's contribution to equilibrium warming (8% of the ECS as quantified for CMIP5 models by Vial et al. 2013). Recognizing this physiological component of CO_2 forcing is necessary for understanding forcing differences across greenhouse gases (e.g. CH_4 does not have added warming from physiology). While the contribution of the physiological effect can be up to 20% of the total TCR in some CMIP5 models, changes in the representation of plant physiology do not appear to be a major driver of the increase in the TCR observed from CMIP5 to CMIP6.

4.2. Physiology's Role in Forcing, Feedbacks, and ECS

The effective radiative forcing is commonly expressed as a change in net top-of-atmosphere (TOA) radiation following CO_2-driven adjustments in tropospheric and stratospheric temperatures, water vapor, clouds, and surface properties, prior to any global-mean surface temperature change (e.g. Boucher et al. 2013; Sherwood et al. 2015). In practice, it is often calculated using simulations in which CO_2 is increased while sea-surface temperatures (SSTs) are prescribed to be fixed at pre-industrial values, with some studies estimating and removing the TOA radiative response to land warming when calculating the forcing value (Hansen et al. 2005; Vial et al. 2013; Tang et al. 2019). Meanwhile, radiative feedbacks are traditionally defined by the change in net TOA radiation for a given change in global-mean surface temperature (Bony et al. 2006; Roe 2009).

523 The physiological response of plants to increasing CO_2 poses a challenge to this
524 radiative forcing–feedback paradigm. On the one hand, plants respond directly to the
525 atmospheric CO_2 concentration, suggesting that the physiological effect should be
526 classified as part of the forcing. However, because this direct physiological response of
527 plants to CO_2 induces changes in surface temperature (even in the absence of the
528 radiative effects of CO_2 changes), the TOA radiative response to these changes could
529 also be classified as part of the feedback. Meanwhile, temperature-driven changes in
530 vegetation distribution and leaf area that influence land surface albedo and
531 evapotranspiration should clearly be classified as feedbacks. While it is unclear to us
532 how best to interpret the physiological effect in terms of the forcing–feedback paradigm,
533 the distinction does not impact the results presented here because of our results' focus
534 on the TCR instead of forcing or feedbacks separately.
535 However, understanding of the role of the physiological effect in TCR and ECS
536 uncertainty would benefit from greater clarity on whether it should be treated as a
537 forcing or feedback. Indeed, recent work suggests that the TCR may be more sensitive
538 to uncertainty in CO_2 radiative forcing than to uncertainty in radiative feedbacks
539 (Lutsko and Popp 2019), but that the ECS is more sensitive to uncertainty in radiative
540 feedbacks (Geoffroy et al. 2012). Thus, while the results here suggest that the
541 physiological effect will act to increase the ECS and its uncertainty – as it has for the
542 TCR – we cannot currently quantify the magnitude of the effect on the ECS in the
543 CMIP5 or CMIP6 ensembles. Additional RAD and PHYS simulations for abrupt CO_2
544 quadrupling, using both fixed SSTs[1] to be able to quantify the effective radiative forcing

[1] For example, the CMIP6 Cloud Feedback Model Intercomparison Project (CFMIP; Webb et al. 2017) tier 2 experiment piSST-4xCO2-rad, in which SSTs are fixed at pre-industrial levels and only the radiation scheme (and not the vegetation scheme) experience an abrupt quadrupling of CO_2

and coupled model simulations to be able to estimate ECS, would be valuable in this regard.

4.3. Broad Implications of Carbon Cycle Uncertainty

While we report physiology's mean contribution to warming, we especially emphasize our finding that uncertainty in terrestrial carbon cycle processes contributes to uncertainty in CO_2-forced warming. The spread in the magnitude of physiologically-driven warming across CMIP6 models represents real scientific uncertainty, as there are limited observational constraints to suggest that either the high or low extremes of modeled physiological responses of stomatal conductance, leaf area, and resulting evapotranspiration are within expectations (Medlyn et al. 2011; De Kauwe et al. 2013; Schimel et al. 2015).

It is also possible that ESMs do not probe the full scientific uncertainty surrounding plants' responses to CO_2, as models may contain systematic biases. For example, many models represent stomatal conductance using the same key parameters (e.g. the same slope constant in the Ball-Berry (1987) stomatal conductance model or the g1 fitted parameter in the Medlyn (2011) model) to govern how stomatal conductance responds to increasing CO_2, despite the wide variation in these parameters across and within plant functional types (Lin et al. 2015; Wolz et al. 2017). Similarly, some studies suggest (e.g. Smith et al. 2016) that ESMs systematically overestimate the leaf area increases resulting from CO_2 fertilization, which would mean that models overestimate physiologically-driven albedo decreases and underestimate physiologically-driven evapotranspiration decreases. We would expect this to result in a true physiologically-forced temperature change that is smaller than models suggest at high latitudes (where albedo matters more) and larger than models suggest at low latitudes (where ET matters more). Furthermore, Green et al. (2017) suggest that ESMs may

570 systematically underestimate some feedbacks between land biosphere changes and the
571 atmosphere.
572 On the one hand, acknowledging the physiological contribution to uncertainty in
573 modeled CO_2-forced warming suggests that models agree more on the magnitude of
574 radiatively forced warming than the prevailing narrative implies. For atmospheric
575 dynamicists most interested in purely radiatively-driven processes, these findings
576 therefore motivate more deliberate consideration of plant functioning in experimental
577 designs; RAD simulations may be more appropriate than FULL simulations for some
578 climate dynamics questions. On the other hand, acknowledging the physiological
579 contribution means that reducing uncertainty in the true, full TCR requires reducing
580 uncertainty in land surface processes which are especially difficult to constrain. From
581 this perspective, these findings provide a new motivation for further experimental
582 studies to reduce uncertainty in terrestrial carbon cycle processes. For example, we
583 identify that plants' responses to CO_2 are a major driver of uncertainty in transient
584 warming in tropical Africa, and no free-air CO_2 enrichment (FACE) experiments exist
585 in tropical forests to constrain uncertainty in how those ecosystems will respond to
586 increasing CO_2. Carbon cycle uncertainty is not limited to the carbon cycle, and
587 reducing uncertainty in plants' response to CO_2 will improve our understanding of
588 physiological warming, thereby reducing overall uncertainty in the total TCR.
589

590 # 5. Data and Code Availability

591 The majority of model output data used in this study are available in the
592 publicly accessible Earth System Grid Federation (ESGF) repository at https://esgf-
593 node.llnl.gov/projects/esgf-llnl/. Model output from the CESM2 RAD experiment is not
594 yet available on the ESGF repository and is stored on data servers at the National

Center for Atmospheric Research. The code used for this study is available from the corresponding author upon request.

6. Acknowledgements

CMZ was supported by the University of Washington Program on Climate Change Fellowship and the Department of Energy Computational Science Graduate Fellowship (DE-SC0020347). MML was supported by the James S. McDonnell Foundation. ALS, MLL, and CMZ were supported by the National Science Foundation AGS-1553715 to the University of Washington. KCA was supported by the National Science Foundation AGS-1752796 to the University of Washington. JTR acknowledges support from the RUBISCO Scientific Focus Area that receives funding from the Regional and Global Modeling program within the Biological and Environmental Research division of DOE's Office of Science. We acknowledge the organizations responsible for CMIP, including the climate modeling groups that participated in C4MIP and shared their model output by uploading it to the Earth System Grid Federation.

7. References

Anav, A., and Coauthors, 2013: Evaluating the Land and Ocean Components of the Global Carbon Cycle in the CMIP5 Earth System Models. *J. Clim.*, **26**, https://doi.org/10.1175/JCLI-D-12-00417.1.

Andrews, T., P. M. Forster, and J. M. Gregory, 2009: A Surface Energy Perspective on Climate Change. *J. Clim.*, **22**, 2557–2570, https://doi.org/10.1175/2008JCLI2759.1.

——, M. Doutriaux-Boucher, O. Boucher, and P. M. Forster, 2011: A regional and global analysis of carbon dioxide physiological forcing and its impact on climate. *Clim. Dyn.*, **36**, 783–792, https://doi.org/10.1007/s00382-010-0742-1.

——, M. A. Ringer, M. Doutriaux-Boucher, M. J. Webb, and W. J. Collins, 2012: Sensitivity of an Earth system climate model to idealized radiative forcing. *Geophys. Res. Lett.*, **39**, https://doi.org/10.1029/2012GL051942.

——, and Coauthors, 2019: Forcings, Feedbacks, and Climate Sensitivity in HadGEM3-GC3.1 and UKESM1. *J. Adv. Model. Earth Syst.*, **n/a**, https://doi.org/10.1029/2019MS001866.

Arellano, J. V.-G. de, C. C. van Heerwaarden, and J. Lelieveld, 2012: Modelled suppression of boundary-layer clouds by plants in a CO 2 -rich atmosphere. *Nat. Geosci.*, **5**, 701–704, https://doi.org/10.1038/ngeo1554.

Arora, V. K., and Coauthors, 2013: Carbon–Concentration and Carbon–Climate Feedbacks in CMIP5 Earth System Models. *J. Clim.*, **26**, 5289–5314, https://doi.org/10.1175/JCLI-D-12-00494.1.

——, and Coauthors, 2019: Carbon-concentration and carbon-climate feedbacks in CMIP6 models, and their comparison to CMIP5 models. *Biogeosciences Discuss.*, https://doi.org/10.5194/bg-2019-473.

Bala, G., K. Caldeira, A. Mirin, M. Wickett, C. Delire, and T. J. Phillips, 2006: Biogeophysical effects of CO2 fertilization on global climate. *Tellus B*, **58**, 620–627, https://doi.org/10.1111/j.1600-0889.2006.00210.x.

Ball, J. T., I. E. Woodrow, and J. A. Berry, 1987: A Model Predicting Stomatal Conductance and its Contribution to the Control of Photosynthesis under

Different Environmental Conditions. *Progress in Photosynthesis Research*, J. Biggins, Ed., Springer Netherlands, 221–224.

Betts, R. A., 2000: Offset of the potential carbon sink from boreal forestation by decreases in surface albedo. *Nature*, **408**, 187–190, https://doi.org/10.1038/35041545.

——, P. M. Cox, S. E. Lee, and F. I. Woodward, 1997: Contrasting physiological and structural vegetation feedbacks in climate change simulations. *Nature*, **387**, 796–799, https://doi.org/10.1038/42924.

——, and Coauthors, 2007: Projected increase in continental runoff due to plant responses to increasing carbon dioxide. *Nature*, **448**, 1037–1041, https://doi.org/10.1038/nature06045.

Bony, S., and Coauthors, 2006: How Well Do We Understand and Evaluate Climate Change Feedback Processes? *J. Clim.*, **19**, 3445–3482, https://doi.org/10.1175/JCLI3819.1.

Boucher, O., A. Jones, and R. A. Betts, 2009: Climate response to the physiological impact of carbon dioxide on plants in the Met Office Unified Model HadCM3. *Clim. Dyn.*, **32**, 237–249, https://doi.org/10.1007/s00382-008-0459-6.

——, and Coauthors, 2013: Clouds and aerosols. *Climate change 2013: the physical science basis. Contribution of Working Group I to the Fifth Assessment Report of the Intergovernmental Panel on Climate Change*.

Bounoua, L., and Coauthors, 1999: Interactions between Vegetation and Climate: Radiative and Physiological Effects of Doubled Atmospheric CO2. *J. Clim.*, **12**, 309–324, https://doi.org/10.1175/1520-0442(1999)012<0309:IBVACR>2.0.CO;2.

Byrne, M. P., and P. A. O'Gorman, 2016: Understanding Decreases in Land Relative Humidity with Global Warming: Conceptual Model and GCM Simulations. *J. Clim.*, **29**, 9045–9061, https://doi.org/10.1175/JCLI-D-16-0351.1.

——, and ——, 2018: Trends in continental temperature and humidity directly linked to ocean warming. *Proc. Natl. Acad. Sci.*, **115**, 4863–4868, https://doi.org/10.1073/pnas.1722312115.

Caesar, L., S. Rahmstorf, A. Robinson, G. Feulner, and V. Saba, 2018: Observed fingerprint of a weakening Atlantic Ocean overturning circulation. *Nature*, **556**, 191–196, https://doi.org/10.1038/s41586-018-0006-5.

Cao, L., G. Bala, K. Caldeira, R. Nemani, and G. Ban-Weiss, 2009: Climate response to physiological forcing of carbon dioxide simulated by the coupled Community Atmosphere Model (CAM3.1) and Community Land Model (CLM3.0). *Geophys. Res. Lett.*, **36**, https://doi.org/10.1029/2009GL037724.

——, ——, ——, ——, and G. Ban-Weiss, 2010: Importance of carbon dioxide physiological forcing to future climate change. *Proc. Natl. Acad. Sci.*, **107**, 9513–9518, https://doi.org/10.1073/pnas.0913000107.

Collatz, G. J., L. Bounoua, S. O. Los, D. A. Randall, I. Y. Fung, and P. J. Sellers, 2000: A mechanism for the influence of vegetation on the response of the diurnal temperature range to changing climate. *Geophys. Res. Lett.*, **27**, 3381–3384, https://doi.org/10.1029/1999GL010947.

Cox, P. M., R. A. Betts, C. B. Bunton, R. L. H. Essery, P. R. Rowntree, and J. Smith, 1999: The impact of new land surface physics on the GCM simulation of climate

and climate sensitivity. *Clim. Dyn.*, **15**, 183–203, https://doi.org/10.1007/s003820050276.

De Kauwe, M. G., and Coauthors, 2013: Forest water use and water use efficiency at elevated CO2: a model-data intercomparison at two contrasting temperate forest FACE sites. *Glob. Change Biol.*, **19**, 1759–1779, https://doi.org/10.1111/gcb.12164.

Devaraju, N., G. Bala, and A. Modak, 2015: Effects of large-scale deforestation on precipitation in the monsoon regions: Remote versus local effects. *Proc. Natl. Acad. Sci.*, **112**, 3257–3262, https://doi.org/10.1073/pnas.1423439112.

——, N. de Noblet-Ducoudré, B. Quesada, and G. Bala, 2018: Quantifying the Relative Importance of Direct and Indirect Biophysical Effects of Deforestation on Surface Temperature and Teleconnections. *J. Clim.*, **31**, 3811–3829, https://doi.org/10.1175/JCLI-D-17-0563.1.

Diffenbaugh, N. S., M. A. Snyder, and L. C. Sloan, 2004: Could CO2-induced land-cover feedbacks alter near-shore upwelling regimes? *Proc. Natl. Acad. Sci.*, **101**, 27–32, https://doi.org/10.1073/pnas.0305746101.

Dong, B., J. M. Gregory, and R. T. Sutton, 2009: Understanding Land–Sea Warming Contrast in Response to Increasing Greenhouse Gases. Part I: Transient Adjustment. *J. Clim.*, **22**, 3079–3097, https://doi.org/10.1175/2009JCLI2652.1.

Donohue, R. J., M. L. Roderick, T. R. McVicar, and G. D. Farquhar, 2013: Impact of CO2 fertilization on maximum foliage cover across the globe's warm, arid environments. *Geophys. Res. Lett.*, **40**, 3031–3035, https://doi.org/10.1002/grl.50563.

711 Doutriaux-Boucher, M., M. J. Webb, J. M. Gregory, and O. Boucher, 2009: Carbon
712 dioxide induced stomatal closure increases radiative forcing via a rapid reduction
713 in low cloud. *Geophys. Res. Lett.*, **36**, https://doi.org/10.1029/2008GL036273.

714 Douville, H., S. Planton, J.-F. Royer, D. B. Stephenson, S. Tyteca, L. Kergoat, S.
715 Lafont, and R. A. Betts, 2000: Importance of vegetation feedbacks in doubled-
716 CO2 climate experiments. *J. Geophys. Res. Atmospheres*, **105**, 14841–14861,
717 https://doi.org/10.1029/1999JD901086.

718 Field, C. B., R. B. Jackson, and H. A. Mooney, 1995: Stomatal responses to increased
719 CO2: implications from the plant to the global scale. *Plant Cell Environ.*, **18**,
720 1214–1225, https://doi.org/10.1111/j.1365-3040.1995.tb00630.x.

721 Fisher, R. A., and Coauthors, 2019: Parametric Controls on Vegetation Responses to
722 Biogeochemical Forcing in the CLM5. *J. Adv. Model. Earth Syst.*,
723 https://doi.org/10.1029/2019MS001609.

724 Flynn, C. M., and T. Mauritsen, 2020: On the Climate Sensitivity and Historical
725 Warming Evolution in Recent Coupled Model Ensembles. *Atmospheric Chem.*
726 *Phys. Discuss.*, https://doi.org/10.5194/acp-2019-1175.

727 Friedlingstein, P., and Coauthors, 2006: Climate–Carbon Cycle Feedback Analysis:
728 Results from the C4MIP Model Intercomparison. *J. Clim.*, **19**, 3337–3353,
729 https://doi.org/10.1175/JCLI3800.1.

730 Geoffroy, O., D. Saint-Martin, and A. Ribes, 2012: Quantifying the sources of spread in
731 climate change experiments. *Geophys. Res. Lett.*, **39**,
732 https://doi.org/10.1029/2012GL054172.

733 Gettelman, A., and Coauthors, 2019: High Climate Sensitivity in the Community Earth
734 System Model Version 2 (CESM2). *Geophys. Res. Lett.*, **46**, 8329–8337,
735 https://doi.org/10.1029/2019GL083978.

736 Golaz, J.-C., and Coauthors, 2019: The DOE E3SM Coupled Model Version 1: Overview
737 and Evaluation at Standard Resolution. *J. Adv. Model. Earth Syst.*, **11**, 2089–
738 2129, https://doi.org/10.1029/2018MS001603.

739 Green, J. K., A. G. Konings, S. H. Alemohammad, J. Berry, D. Entekhabi, J. Kolassa,
740 J.-E. Lee, and P. Gentine, 2017: Regionally strong feedbacks between the
741 atmosphere and terrestrial biosphere. *Nat. Geosci.*, **10**, 410–414,
742 https://doi.org/10.1038/ngeo2957.

743 Gregory, J. M., and P. M. Forster, 2008: Transient climate response estimated from
744 radiative forcing and observed temperature change. *J. Geophys. Res.*
745 *Atmospheres*, **113**, https://doi.org/10.1029/2008JD010405.

746 ——, and Coauthors, 2004: A new method for diagnosing radiative forcing and climate
747 sensitivity. *Geophys. Res. Lett.*, **31**, https://doi.org/10.1029/2003GL018747.

748 Hansen, J., and Coauthors, 2005: Efficacy of climate forcings. *J. Geophys. Res.*
749 *Atmospheres*, **110**, https://doi.org/10.1029/2005JD005776.

750 Hense, I., I. Stemmler, and S. Sonntag, 2017: Ideas and perspectives: climate-relevant
751 marine biologically driven mechanisms in Earth system models. *Biogeosciences*,
752 **14**, 403–413, https://doi.org/10.5194/bg-14-403-2017.

753 Hungate, B. A., M. Reichstein, P. Dijkstra, D. Johnson, G. Hymus, J. D. Tenhunen, C.
754 R. Hinkle, and B. G. Drake, 2002: Evapotranspiration and soil water content in a

scrub-oak woodland under carbon dioxide enrichment. *Glob. Change Biol.*, **8**, 289–298, https://doi.org/10.1046/j.1365-2486.2002.00468.x.

Jones, C. D., and Coauthors, 2016: C4MIP -- The Coupled Climate–Carbon Cycle Model Intercomparison Project: experimental protocol for CMIP6. *Geosci. Model Dev.*, **9**, 2853–2880, https://doi.org/10.5194/gmd-9-2853-2016.

Joshi, M. M., J. M. Gregory, M. J. Webb, D. M. H. Sexton, and T. C. Johns, 2008: Mechanisms for the land/sea warming contrast exhibited by simulations of climate change. *Clim. Dyn.*, **30**, 455–465, https://doi.org/10.1007/s00382-007-0306-1.

Kooperman, G. J., Y. Chen, F. M. Hoffman, C. D. Koven, K. Lindsay, M. S. Pritchard, A. L. S. Swann, and J. T. Randerson, 2018: Forest response to rising CO2 drives zonally asymmetric rainfall change over tropical land. *Nat. Clim. Change*, **8**, 434–440, https://doi.org/10.1038/s41558-018-0144-7.

Laguë, M. M., and A. L. S. Swann, 2016: Progressive Midlatitude Afforestation: Impacts on Clouds, Global Energy Transport, and Precipitation. *J. Clim.*, **29**, 5561–5573, https://doi.org/10.1175/JCLI-D-15-0748.1.

——, G. B. Bonan, and A. L. S. Swann, 2019: Separating the Impact of Individual Land Surface Properties on the Terrestrial Surface Energy Budget in both the Coupled and Uncoupled Land–Atmosphere System. *J. Clim.*, **32**, 5725–5744, https://doi.org/10.1175/JCLI-D-18-0812.1.

Langenbrunner, B., M. S. Pritchard, G. J. Kooperman, and J. T. Randerson, 2019: Why Does Amazon Precipitation Decrease When Tropical Forests Respond to

Increasing CO2? *Earths Future*, **7**, 450–468, https://doi.org/10.1029/2018EF001026.

Leakey, A. D. B., E. A. Ainsworth, C. J. Bernacchi, A. Rogers, S. P. Long, and D. R. Ort, 2009: Elevated CO2 effects on plant carbon, nitrogen, and water relations: six important lessons from FACE. *J. Exp. Bot.*, **60**, 2859–2876, https://doi.org/10.1093/jxb/erp096.

Leeuwen, T. T. van, A. J. Frank, Y. Jin, P. Smyth, M. L. Goulden, G. R. van der Werf, and J. T. Randerson, 2011: Optimal use of land surface temperature data to detect changes in tropical forest cover. *J. Geophys. Res. Biogeosciences*, **116**, https://doi.org/10.1029/2010JG001488.

Lemordant, L., and P. Gentine, 2019: Vegetation Response to Rising CO2 Impacts Extreme Temperatures. *Geophys. Res. Lett.*, **46**, 1383–1392, https://doi.org/10.1029/2018GL080238.

——, ——, M. Stéfanon, P. Drobinski, and S. Fatichi, 2016: Modification of land-atmosphere interactions by CO2 effects: Implications for summer dryness and heat wave amplitude. *Geophys. Res. Lett.*, **43**, 10,240-10,248, https://doi.org/10.1002/2016GL069896.

——, ——, A. S. Swann, B. I. Cook, and J. Scheff, 2018: Critical impact of vegetation physiology on the continental hydrologic cycle in response to increasing CO2. *Proc. Natl. Acad. Sci.*, **115**, 4093–4098, https://doi.org/10.1073/pnas.1720712115.

Levis, S., J. A. Foley, and D. Pollard, 2000: Large-Scale Vegetation Feedbacks on a Doubled CO2 Climate. *J. Clim.*, **13**, 1313–1325, https://doi.org/10.1175/1520-0442(2000)013<1313:LSVFOA>2.0.CO;2.

Lian, X., and Coauthors, 2018: Partitioning global land evapotranspiration using CMIP5 models constrained by observations. *Nat. Clim. Change*, **8**, 640–646, https://doi.org/10.1038/s41558-018-0207-9.

Lin, Y.-S., and Coauthors, 2015: Optimal stomatal behaviour around the world. *Nat. Clim. Change*, **5**, 459–464, https://doi.org/10.1038/nclimate2550.

Lutsko, N. J., and M. Popp, 2019: Probing the Sources of Uncertainty in Transient Warming on Different Timescales. *Geophys. Res. Lett.*, **46**, 11367–11377, https://doi.org/10.1029/2019GL084018.

Marshall, J., J. R. Scott, K. C. Armour, J.-M. Campin, M. Kelley, and A. Romanou, 2015: The ocean's role in the transient response of climate to abrupt greenhouse gas forcing. *Clim. Dyn.*, **44**, 2287–2299, https://doi.org/10.1007/s00382-014-2308-0.

Medlyn, B. E., and Coauthors, 2011: Reconciling the optimal and empirical approaches to modelling stomatal conductance. *Glob. Change Biol.*, **17**, 2134–2144, https://doi.org/10.1111/j.1365-2486.2010.02375.x.

Norby, R. J., and D. R. Zak, 2011: Ecological Lessons from Free-Air CO2 Enrichment (FACE) Experiments. *Annu. Rev. Ecol. Evol. Syst.*, **42**, 181–203, https://doi.org/10.1146/annurev-ecolsys-102209-144647.

O'ishi, R., A. Abe-Ouchi, I. C. Prentice, and S. Sitch, 2009: Vegetation dynamics and plant CO2 responses as positive feedbacks in a greenhouse world. *Geophys. Res. Lett.*, **36**, https://doi.org/10.1029/2009GL038217.

821 Parsons, L. A., K. Brennan, R. Jnglin Wills, and C. Proistosescu, In Revision:
822 Magnitudes and spatial patterns of interdecadal temperature variability in
823 CMIP6. *Geophys. Res. Lett.*,.

824 Piao, S., and Coauthors, 2013: Evaluation of terrestrial carbon cycle models for their
825 response to climate variability and to CO2 trends. *Glob. Change Biol.*, **19**, 2117–
826 2132, https://doi.org/10.1111/gcb.12187.

827 Pu, B., and R. E. Dickinson, 2012: Examining vegetation feedbacks on global warming
828 in the Community Earth System Model. *J. Geophys. Res. Atmospheres*, **117**,
829 https://doi.org/10.1029/2012JD017623.

830 Roe, G., 2009: Feedbacks, Timescales, and Seeing Red. *Annu. Rev. Earth Planet. Sci.*,
831 **37**, 93–115, https://doi.org/10.1146/annurev.earth.061008.134734.

832 Schimel, D., B. B. Stephens, and J. B. Fisher, 2015: Effect of increasing CO2 on the
833 terrestrial carbon cycle. *Proc. Natl. Acad. Sci.*, **112**, 436–441,
834 https://doi.org/10.1073/pnas.1407302112.

835 Sellers, P. J., and Coauthors, 1996: Comparison of Radiative and Physiological Effects
836 of Doubled Atmospheric CO2 on Climate. *Science*, **271**, 1402–1406,
837 https://doi.org/10.1126/science.271.5254.1402.

838 Sherwood, S. C., S. Bony, O. Boucher, C. Bretherton, P. M. Forster, J. M. Gregory, and
839 B. Stevens, 2015: Adjustments in the Forcing-Feedback Framework for
840 Understanding Climate Change. *Bull. Am. Meteorol. Soc.*, **96**, 217–228,
841 https://doi.org/10.1175/BAMS-D-13-00167.1.

Skinner, C. B., C. J. Poulsen, and J. S. Mankin, 2018: Amplification of heat extremes by plant CO 2 physiological forcing. *Nat. Commun.*, **9**, 1–11, https://doi.org/10.1038/s41467-018-03472-w.

Smith, W. K., S. C. Reed, C. C. Cleveland, A. P. Ballantyne, W. R. L. Anderegg, W. R. Wieder, Y. Y. Liu, and S. W. Running, 2016: Large divergence of satellite and Earth system model estimates of global terrestrial CO 2 fertilization. *Nat. Clim. Change*, **6**, 306–310, https://doi.org/10.1038/nclimate2879.

Swann, A. L. S., I. Y. Fung, and J. C. H. Chiang, 2012: Mid-latitude afforestation shifts general circulation and tropical precipitation. *Proc. Natl. Acad. Sci.*, **109**, 712–716, https://doi.org/10.1073/pnas.1116706108.

——, ——, Y. Liu, and J. C. H. Chiang, 2014: Remote Vegetation Feedbacks and the Mid-Holocene Green Sahara. *J. Clim.*, **27**, 4857–4870, https://doi.org/10.1175/JCLI-D-13-00690.1.

——, F. M. Hoffman, C. D. Koven, and J. T. Randerson, 2016: Plant responses to increasing CO2 reduce estimates of climate impacts on drought severity. *Proc. Natl. Acad. Sci.*, **113**, 10019–10024, https://doi.org/10.1073/pnas.1604581113.

Tang, T., and Coauthors, 2019: Comparison of Effective Radiative Forcing Calculations Using Multiple Methods, Drivers, and Models. *J. Geophys. Res. Atmospheres*, **124**, 4382–4394, https://doi.org/10.1029/2018JD030188.

Vargas Zeppetello, L. R., A. Donohoe, and D. S. Battisti, 2019: Does Surface Temperature Respond to or Determine Downwelling Longwave Radiation? *Geophys. Res. Lett.*, **46**, 2781–2789, https://doi.org/10.1029/2019GL082220.

Vial, J., J.-L. Dufresne, and S. Bony, 2013: On the interpretation of inter-model spread in CMIP5 climate sensitivity estimates. *Clim. Dyn.*, **41**, 3339–3362, https://doi.org/10.1007/s00382-013-1725-9.

Vico, G., S. Manzoni, S. Palmroth, and G. Katul, 2011: Effects of stomatal delays on the economics of leaf gas exchange under intermittent light regimes. *New Phytol.*, **192**, 640–652, https://doi.org/10.1111/j.1469-8137.2011.03847.x.

Webb, M. J., and Coauthors, 2017: The Cloud Feedback Model Intercomparison Project (CFMIP) contribution to CMIP6. *Geosci. Model Dev.*, **10**, 359–384, https://doi.org/10.5194/gmd-10-359-2017.

Wolz, K. J., T. M. Wertin, M. Abordo, D. Wang, and A. D. B. Leakey, 2017: Diversity in stomatal function is integral to modelling plant carbon and water fluxes. *Nat. Ecol. Evol.*, **1**, 1292–1298, https://doi.org/10.1038/s41559-017-0238-z.

8. Tables

Experiment	CMIP5 Experiment Name	CMIP6 Experiment Name	Influence of CO_2 Concentration on:		
			Land	Ocean	Atmosphere
FULL	1pctCO2	1pctCO2	1% per year	1% per year	1% per year
PHYS	esmFixClim1	1pctCO2-bgc	1% per year	1% per year	Pre-industrial
RAD	exmFdbk1	1pctCO2-rad	Pre-industrial	Pre-industrial	1% per year
PI	piControl	piControl	Pre-industrial	Pre-industrial	Pre-industrial

TABLE 1. Summary of CMIP experiments used.

881

Modeling Center	CMIP5 Model TCR								CMIP6 Model TCR							
	Model Name	FULL	RAD		PHYS-PI		TOT-RAD		Model Name	FULL	RAD		PHYS-PI		TOT-RAD	
		°C	°C	%	°C	%	°C	%		°C	°C	%	°C	%	°C	%
Beijing Climate Center (BCC)	bcc-csm1-1	1.73	1.67	96.5%	0.05	2.8%	0.06	3.5%	BCC-CSM2-MR	1.73	1.66	95.8%	0.54	31.4%	0.07	4.2%
Canadian Centre for Climate Modelling and Analysis (CCCma)	CanESM2	2.34	2.16	92.0%	0.15	6.5%	0.18	8.0%	CanESM5	2.74	2.64	96.2%	0.04	1.5%	0.10	3.8%
National Center for Atmospheric Research (NCAR)	CESM1-BGC	1.68	1.56	93.2%	0.11	6.6%	0.12	6.8%	CESM2	2.06	1.78	86.1%	0.11	5.2%	0.29	13.9%
NOAA Geophysical Fluid Dynamics Laboratory (NOAA-GFDL)	GFDL-ESM2M	1.35	1.35	99.9%	0.05	3.4%	0.00	0.1%	GFDL-ESM4	1.61	1.58	98.6%	0.17	10.7%	0.02	1.4%
Met Office Hadley Centre (MOHC)	HadGEM2-ES	2.52	2.01	79.9%	0.37	14.6%	0.51	20.1%	UKESM1-0-LL	2.79	2.51	90.0%	0.17	6.0%	0.28	10.0%
Institut Pierre Simon Laplace (IPSL)	IPSL-CM5A-LR	2.00	1.97	98.3%	0.11	5.6%	0.03	1.7%	IPSL-CM6A-LR	2.31	2.23	96.4%	0.17	7.3%	0.08	3.6%
Norwegian Climate Centre (NCC)	NorESM1-ME	1.56	1.42	90.8%	0.08	5.3%	0.14	9.2%	-	-	-	-	-	-	-	-
Max Planck Institute for Meteorology (MPI-M)	MPI-ESM-LR	2.02	1.95	96.4%	0.20	9.9%	0.07	3.6%	-	-	-	-	-	-	-	-
Centre National de Recherches Météorologiques (CNRM-CERFACS)	-	-	-	-	-	-	-	-	CNRM-ESM2-1	1.84	1.80	97.5%	-0.15	-8.0%	0.05	2.5%
NASA Goddard Institute for Space Studies (NASA-GISS)	-	-	-	-	-	-	-	-	GISS-E2-1-G	1.82	1.73	95.0%	0.10	5.7%	0.09	5.0%
Japan Agency for Marine-Earth Science and Technology (JAMSTEC)	-	-	-	-	-	-	-	-	MIROC-ES2L	1.55	1.52	97.6%	0.07	4.8%	0.04	2.4%
Mean	**All Models**	**1.90**	**1.76**	**93.4%**	**0.10**	**6.8%**	**0.14**	**6.6%**	**All Models**	**2.05**	**1.94**	**94.8%**	**0.14**	**7.2%**	**0.11**	**5.2%**
	Consistent Model Subset	*1.94*	*1.79*	*93.3%*	*0.14*	*6.6%*	*0.15*	*6.7%*	*Consistent Model Subset*	*2.21*	*2.06*	*93.9%*	*0.20*	*10.4%*	*0.14*	*6.1%*
Standard Deviation	**All Models**	**0.40**	**0.30**	**6.3%**	**0.11**	**3.8%**	**0.16**	**6.3%**	**All Models**	**0.46**	**0.41**	**4.1%**	**0.18**	**10.5%**	**0.10**	**4.1%**
	Consistent Model Subset	*0.44*	*0.31*	*7.2%*	*0.12*	*4.2%*	*0.19*	*7.2%*	*Consistent Model Subset*	*0.50*	*0.45*	*4.8%*	*0.18*	*10.7%*	*0.11*	*4.8%*

882 **TABLE 2.** TCR_{FULL}, TCR_{RAD}, and TCR_{PHYS} by model, where TCR_{PHYS} is calculated by both PHYS-PI and TOT-RAD.
883 The consistent model subset refers to the six models for which the necessary model output is available for both CMIP5 and
884 CMIP6. For the summary statistics in the last four rows, the percentages refer to the mean and standard deviations of the
885 percent contributions across models.

9. Figures

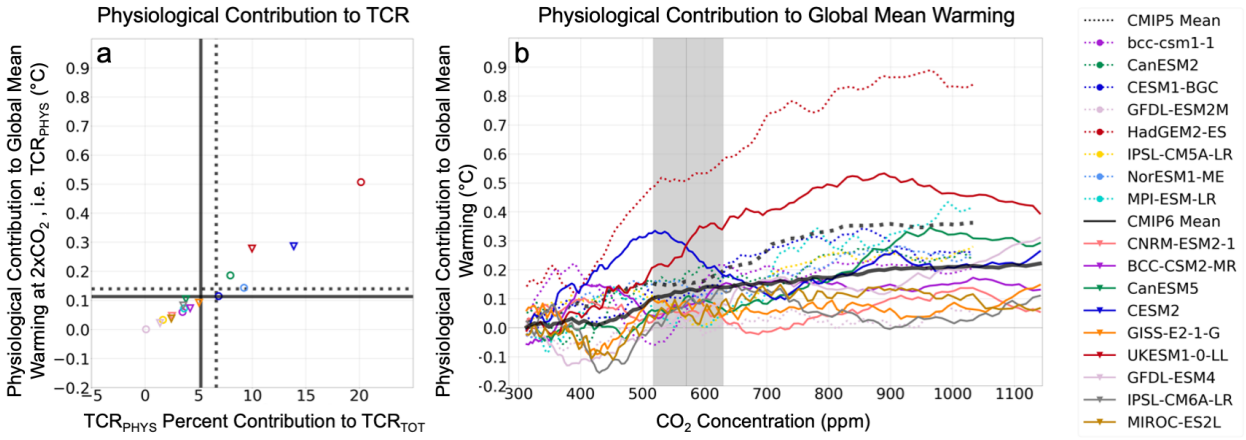

FIGURE 1. Physiological contribution to global mean warming. (a) The relationship between the relative contribution of TCR_{PHYS} to the full TCR (i.e. TCR_{PHYS}/TCR_{FULL}) and the absolute magnitude of TCR_{PHYS}, as calculated by FULL-RAD. Marker types indicate CMIP phase (CMIP5: circles; CMIP6: triangles) and colors indicate modeling center. Lines demarcate the multi-model mean for CMIP5 (dashed) and CMIP6 (solid). Note that the set of models included in the average differs between CMIP5 and CMIP6. (b) Global mean physiologically-driven temperature change as a function of CO_2 concentration, calculated from FULL-RAD and smoothed with a 20-year boxcar. The dark gray vertical line marks the time of CO_2 doubling, and the light gray bar indicates the 20-year period surrounding the time of CO_2 doubling. Colors indicate modeling center as in (a), and line types indicate CMIP phase (CMIP5: dashed; CMIP6: solid).

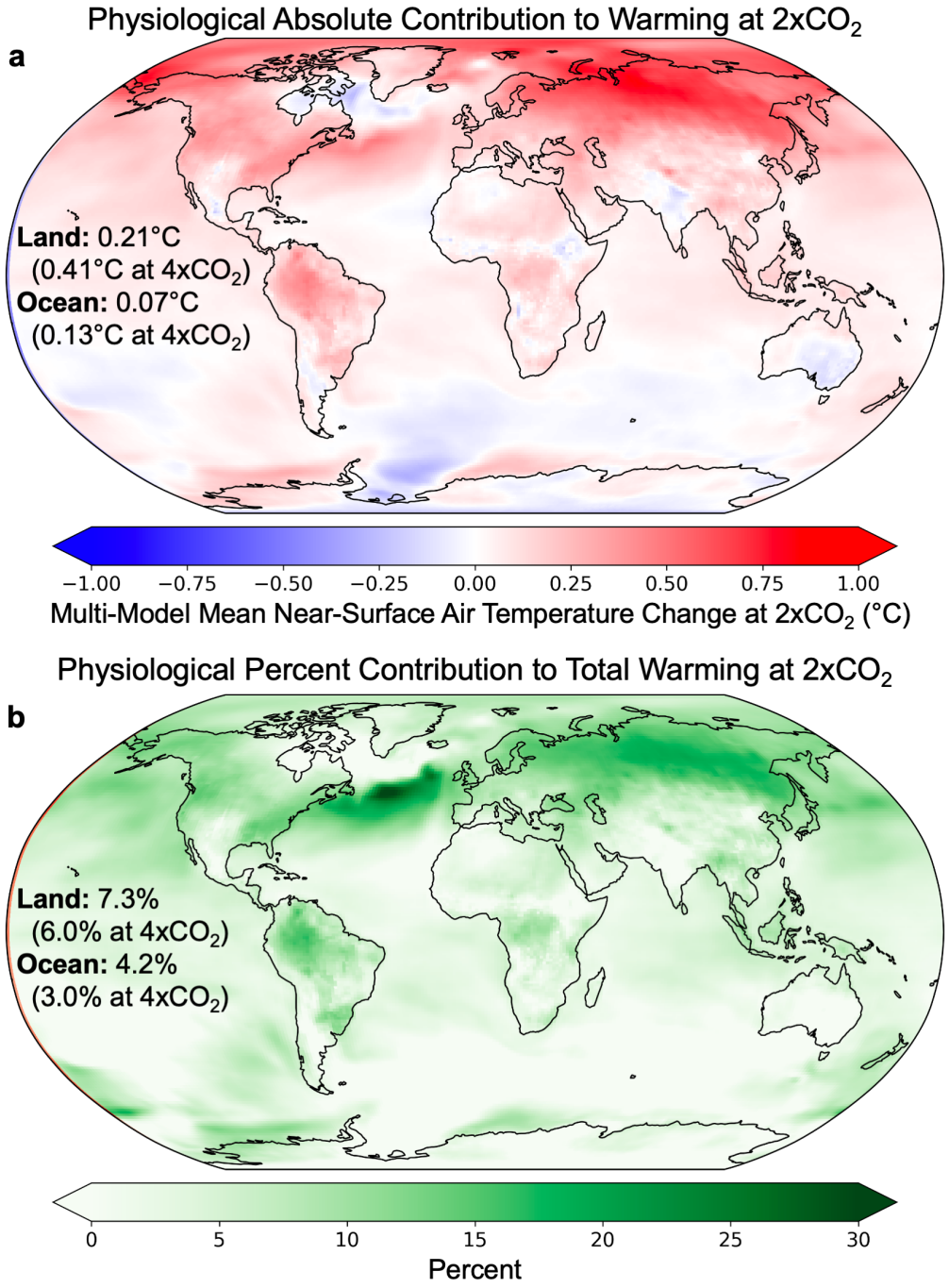

FIGURE 2. Spatial pattern of (a) absolute physiologically-driven warming and (b) physiological percent contribution to total warming at 2xCO_2, where physiologically-driven warming is calculated by FULL-RAD. Multi-model means include the 9 CMIP6 models.

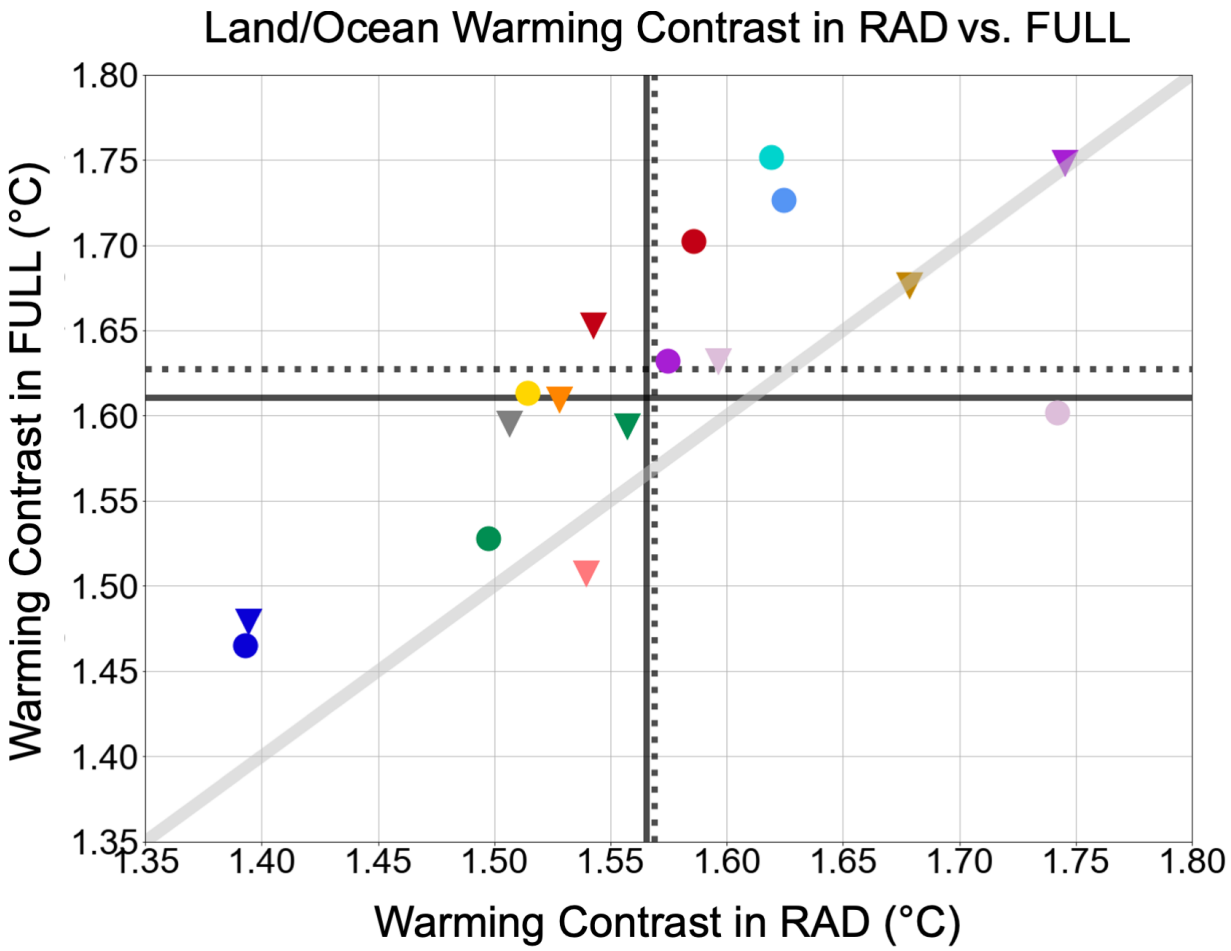

904

905 **FIGURE 3.** The relationship between the land/ocean warming contrast (the ratio of
906 the change in non-glaciated land temperature to the change in ocean temperature) from
907 RAD (RAD-PI) and FULL (FULL-PI). The gray 1:1 line is where we would expect all
908 models to be if the warming contrast were entirely caused by the radiative effects of
909 CO_2. Physiology's addition to the warming contrast is the vertical distance between the
910 gray 1:1 line and each point. Marker types indicate CMIP phase (CMIP5: circles;
911 CMIP6: triangles) and colors indicate modeling center as in Figure 1. Lines demarcate
912 the multi-model average for CMIP5 (dashed) and CMIP6 (solid). Note that the set of
913 models included in the average differs between CMIP5 and CMIP6.

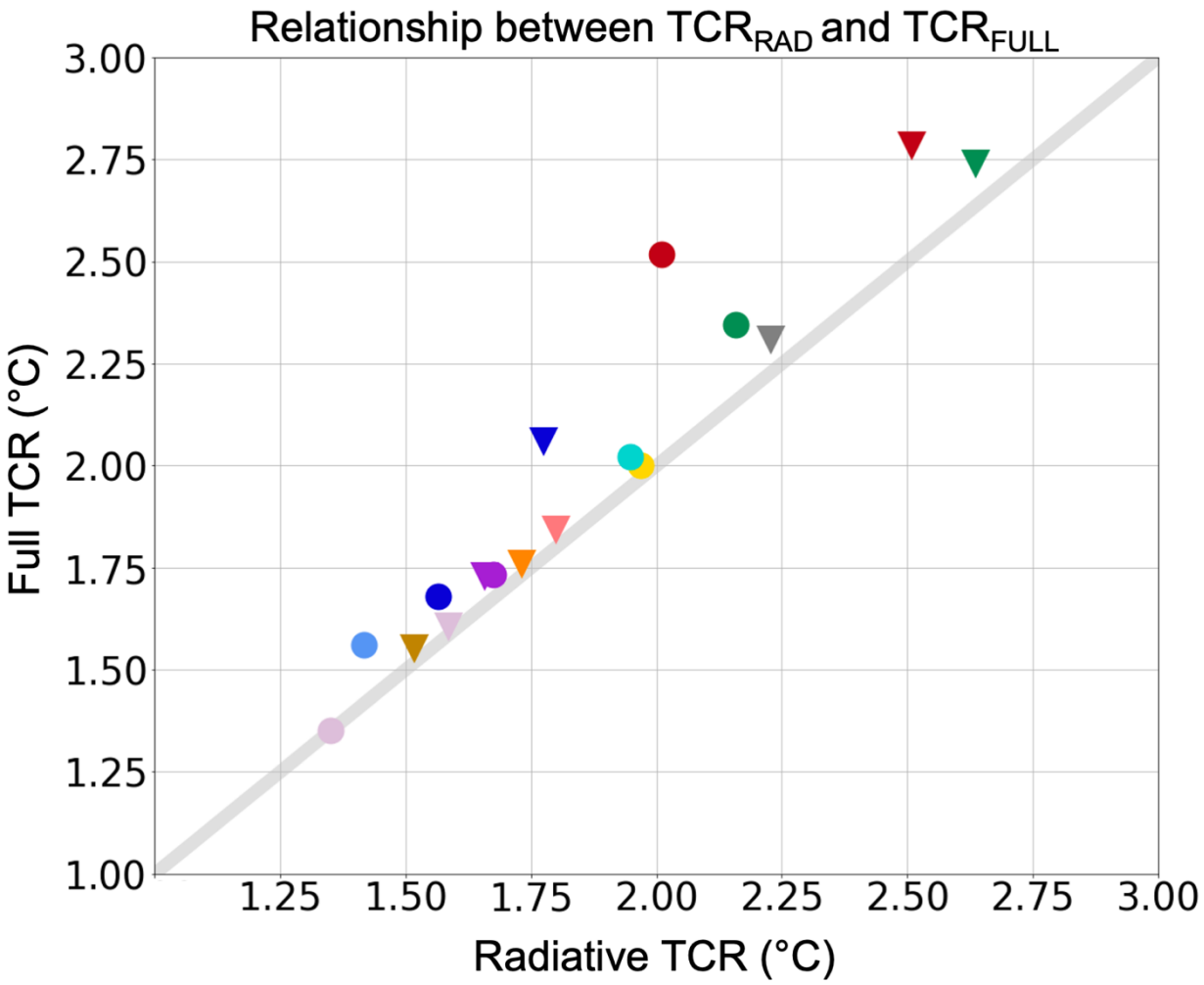

914

915 **FIGURE 4.** The relationship between TCR_{RAD} (RAD-PI) and TCR_{FULL} (FULL-PI).
916 The gray 1:1 line is where we would expect all models to be if the TCR were entirely
917 caused by the radiative effects of CO_2. The added warming from the physiological effect
918 is the vertical distance between the gray 1:1 line and each point. Marker types indicate
919 CMIP phase (CMIP5: circles; CMIP6: triangles) and colors indicate modeling center as
920 in Figure 1.

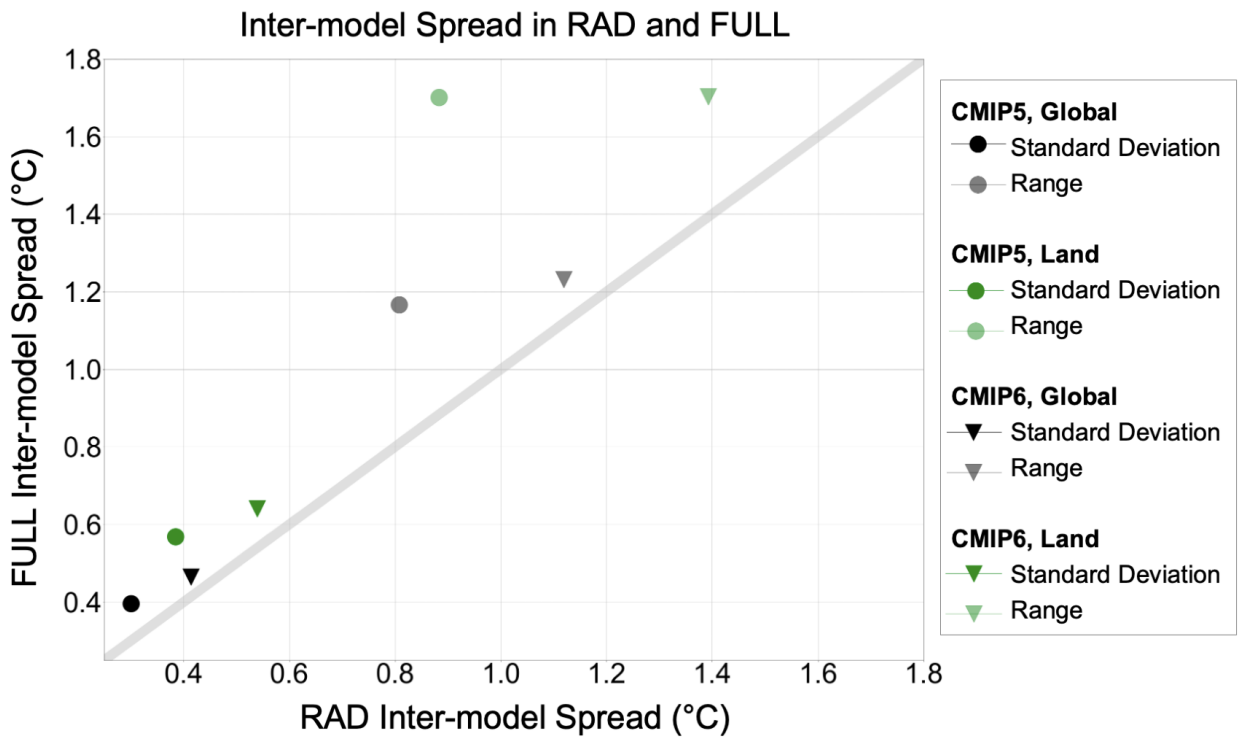

FIGURE 5. Physiology's contribution to inter-model spread in global mean warming. Inter-model spread in global (black and grey) and land only (green) warming in FULL (FULL-PI) and RAD (RAD-PI), as quantified by the full inter-model range and the standard deviation. The 1:1 line is where we would expect all models to be if inter-model spread in warming were entirely caused by the radiative effects of CO_2. The added inter-model spread from the physiological effect is the vertical distance between the gray 1:1 line and each point. Marker types indicate CMIP phase (CMIP5: circles; CMIP6: triangles).

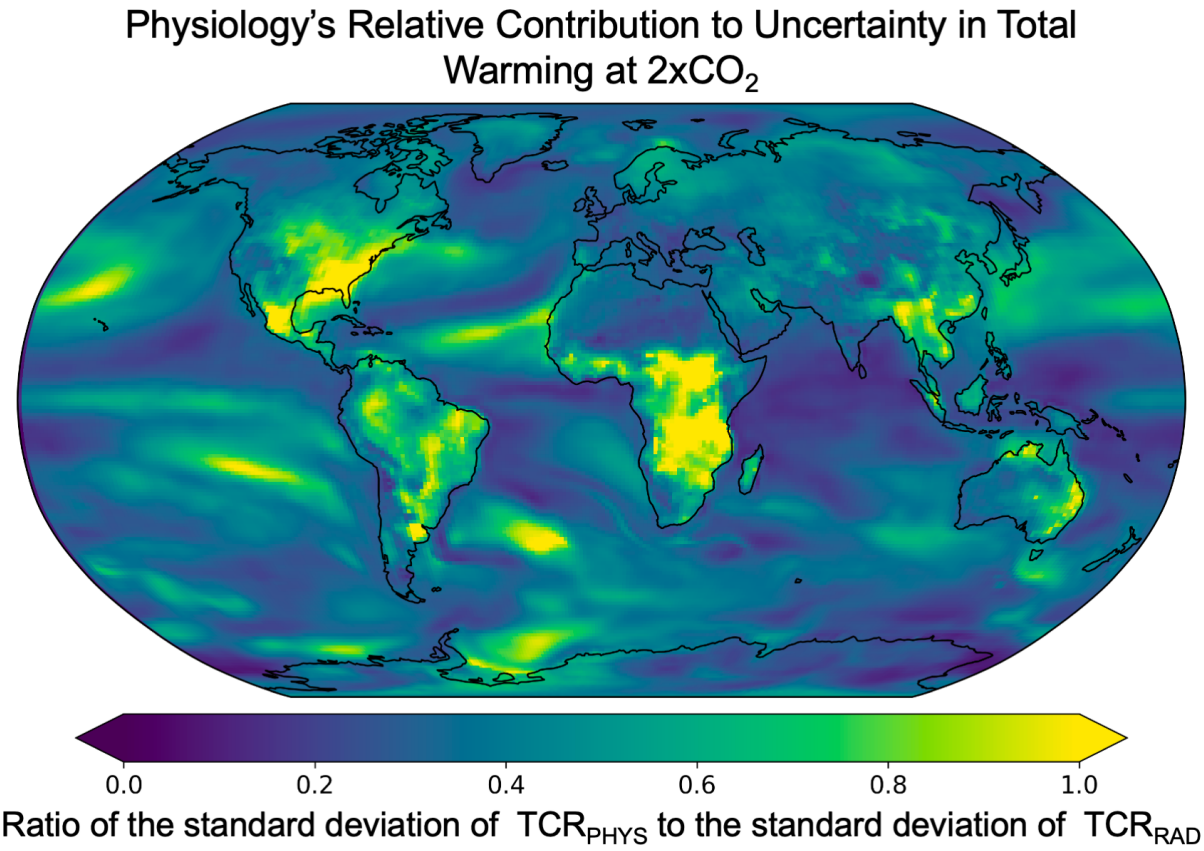

FIGURE 6. Spatial pattern of physiology's relative contribution to inter-model spread in CO_2-forced warming. The ratio of the standard deviation (SD; at each grid cell, across models) of physiologically forced warming (calculated from FULL-RAD) to the SD of radiatively forced warming (calculated from RAD-PI) at 2xCO_2 for CMIP6 models. A value of 1 means that the physiological and radiative effects of CO_2 contribute equally to the total uncertainty in local warming at 2xCO_2 across models.

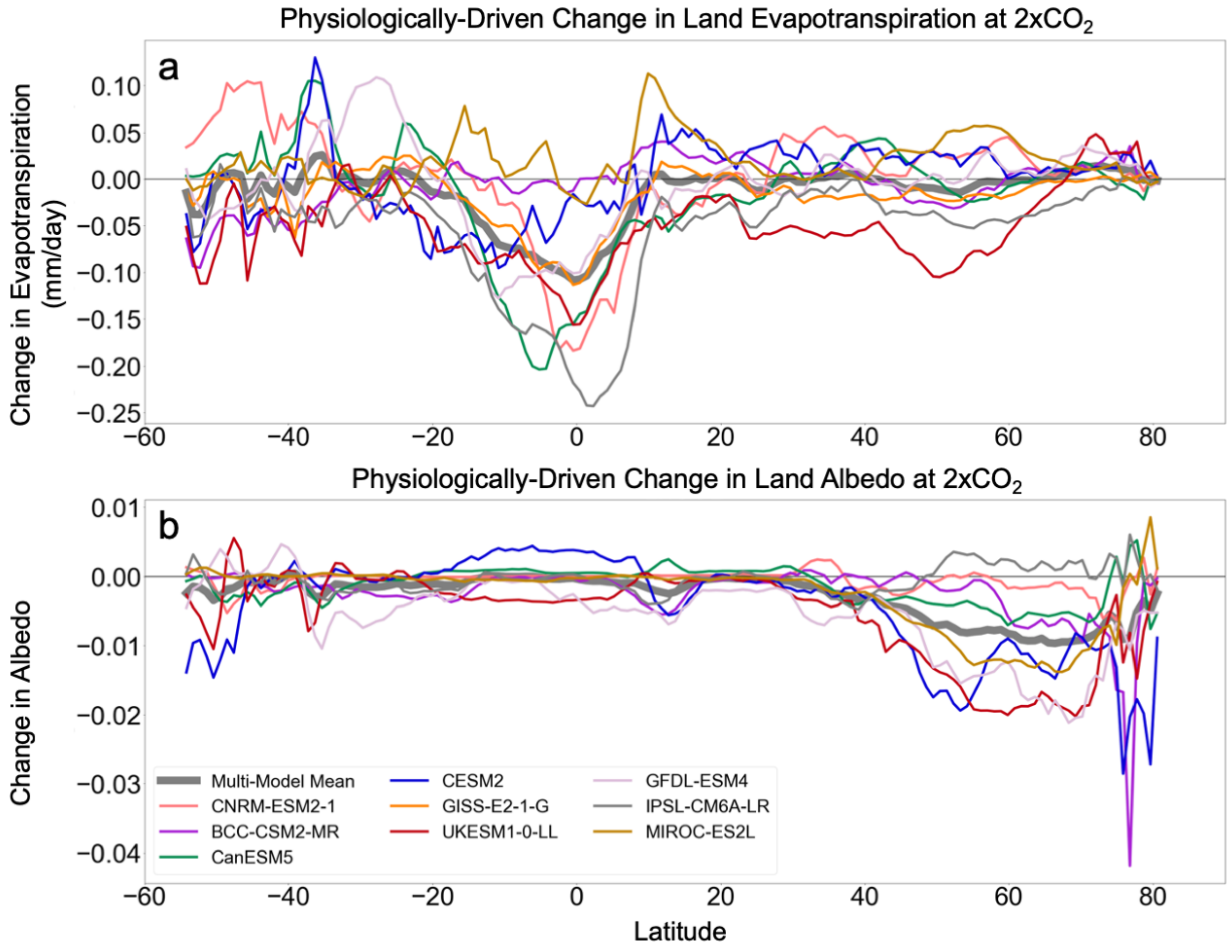

FIGURE 7. Land zonal means of physiologically-driven changes in (a) evapotranspiration and (b) albedo at 2xCO$_2$ for CMIP6 models, as calculated by FULL-RAD.

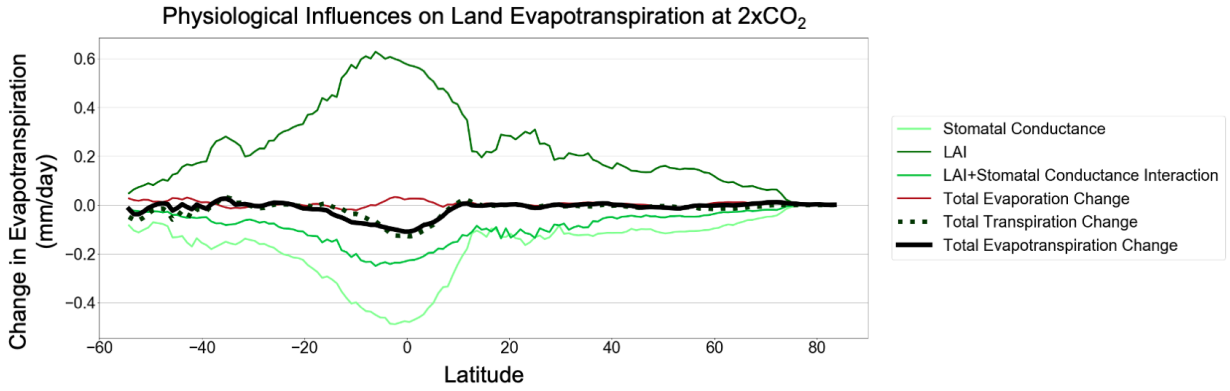

943

944 **FIGURE 8.** Zonal means of how much physiologically-driven changes in different land
945 processes (stomatal conductance, LAI, and evaporation) contribute to the total multi-
946 model mean physiologically-driven change in land evapotranspiration. Multi-model
947 means in this figure are averaged across all CMIP6 models for which model output is
948 available, which consists of up to 9 models. Transpiration and LAI data necessary for
949 this partitioning were not available for GFDL-ESM4, so this model is only included in
950 the multi-model mean for the total evapotranspiration change. The total
951 evapotranspiration change (black line) is the same as the multi-model mean change in
952 evapotranspiration shown in Figure 7a.

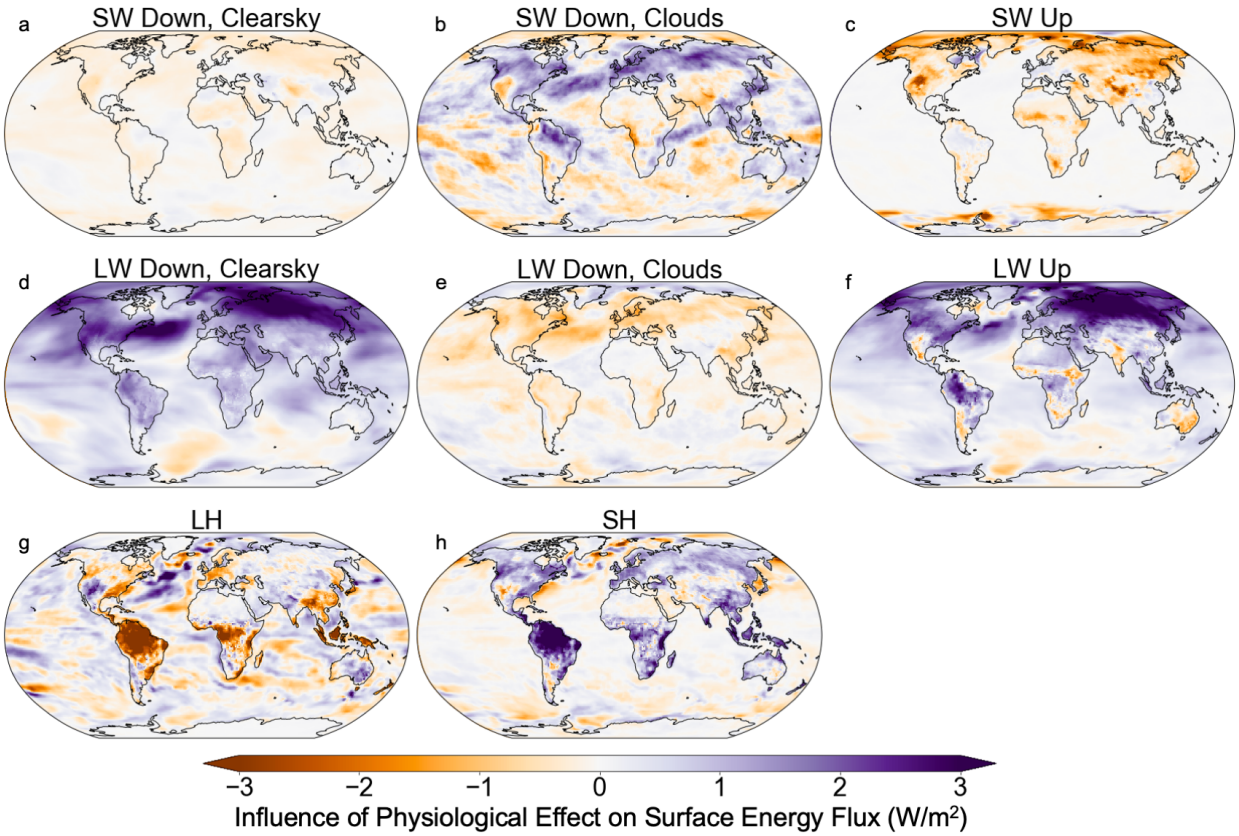

FIGURE 9. Spatial pattern of multi-model mean physiologically-driven changes in surface energy fluxes as calculated by FULL-RAD at the point of CO_2 doubling (averaged over years 61-80) for (a) clear-sky downwelling shortwave radiation, (b) cloudy downwelling shortwave radiation, (c) upwelling shortwave radiation, (d) clear-sky downwelling longwave radiation, (e) cloudy downwelling longwave radiation, (f) upwelling longwave radiation, (g) latent heat, and (h) sensible heat. Multi-model means include all CMIP6 models for which model output is available; this consists of up to 9 models. Data for some surface energy fluxes were not available for the following models: GFDL-ESM4 (panels a, b, d, and e), GISS-E2-1-G, 3 (panels c and h) and CNRM-ESM2-1 (panels d and e).